

18 Mar 2007

Photosensitization of Photoconductive and Photorefractive Composites through the Inclusion of Semiconductor Nanocrystals

Tyler Martin Fears

Follow this and additional works at: <https://scholarsmine.mst.edu/oure>

 Part of the [Physical Chemistry Commons](#)

Recommended Citation

Fears, Tyler Martin, "Photosensitization of Photoconductive and Photorefractive Composites through the Inclusion of Semiconductor Nanocrystals" (2007). *Opportunities for Undergraduate Research Experience Program (OURE)*. 186.

<https://scholarsmine.mst.edu/oure/186>

This Presentation is brought to you for free and open access by Scholars' Mine. It has been accepted for inclusion in Opportunities for Undergraduate Research Experience Program (OURE) by an authorized administrator of Scholars' Mine. This work is protected by U. S. Copyright Law. Unauthorized use including reproduction for redistribution requires the permission of the copyright holder. For more information, please contact scholarsmine@mst.edu.

**Photosensitization of Photoconductive
and Photorefractive Composites through
the Inclusion of Semiconductor
Nanocrystals**

Tyler Martin Fears

Jeffrey G. Winiarz, Professor of Chemistry

3/18/07

Abstract

A novel synthesis of NiS nanocrystals included in photorefractive polymeric composites is described. The nanocrystals were characterized using visible-absorption spectroscopy, energy-dispersive X-ray spectroscopy, and transmission electron microscopy. We further demonstrate the ability to enhance aspects of the composites' photorefractive performance by performing ligand exchange on the nanocrystals prior to their incorporation into the polymer composite. It was originally believed that this modification of the nanocrystals' surface characteristics would result in an enhanced charge-transfer process between the nanocrystal and the charge transporting matrix. However, when the photoconductivities were determined and used in calculating the quantum efficiencies associated with the photorefractive devices, it was determined that this enhancement did not occur.

Introduction

Due to such useful properties as high optical nonlinearity, low permittivity, and low cost, photorefractive polymeric composites are promising materials for a variety of optical processing applications: beam clean-up and amplification, dynamic interferometry, phase conjugation, and pattern recognition.¹⁻⁵ A great deal of research has been focused on this field in the efforts of exploiting these materials, providing many leaps including near 100% diffraction efficiencies.³ By modifying the component parts of these materials, photorefractive composites can be made for specific applications. Normally, a photorefractive composite is composed of a charge-carrying matrix doped with a nonlinear optical dye capable of modulating its refractive index in a space-charge field accompanied by a photosensitizer that can absorb the desired optical wavelength and create free charges.

With the advent of nanotechnology, it has become possible to create organic-inorganic hybrid photorefractive composite materials at new operational wavelengths.⁶⁻¹⁸ Organic photosensitizers are limited on the wavelengths of light at which they can operate, but semiconducting nanocrystals can operate at a wide range of frequencies and are easily tunable.⁶⁻⁹ This tunability is probably the most appealing aspect of hybrid photorefractive materials. In the nano regime, semiconductor band gaps become highly dependent upon particle size, whereas bulk semiconducting materials have well-known band-gaps that remain constant for each material regardless of the particle size. By taking advantage of this property it is possible to blue-shift semiconductor band-gaps by synthesizing smaller nanocrystals.

While these new hybrid materials show enormous promise, they are still not as efficient as their all organic counterparts. Much research is needed to improve these materials to meet the necessary requirements for practical applications. By studying the mechanisms involved in photo-charge generation and charge transport as well as developing new methods for photorefractive device assembly, it can become possible to utilize these hybrid materials in practical applications. Recently, new methods for synthesizing nanocrystalline materials have allowed for a finer control of nanocrystal size, morphology, and composition. With few exceptions,^{10, 13, 14} studies concerning the photosensitization of hybrid photorefractive composites with quantum dots have focused on one of only four semiconductor materials: CdSe, CdS, PbSe and PbS.

In this communication we report on the photoconductive performance of a hybrid composite photosensitized with NiS nanocrystals synthesized based on an approach found in literature.¹⁹ The nanocrystalline particles were characterized by visible-absorption spectroscopy, energy-dispersive X-ray spectroscopy (EDS), and transmission-electron microscopy (TEM). In addition, some of the nanocrystals were modified by ligand exchange, replacing oleic acid (OA) and trioctylphosphine (TOP) with pyridine.

The composites contained poly(*N*-vinylcarbazole) (PVK) as a charge-transporting species, plasticized with *N*-ethylcarbazole (ECZ), doped with the nonlinear dye 4-homopiperidinobenzylidenemalononitrile (7-DCST).^{20, 21} The photoconductive performance of the composites were measured and the interpretation of the results will be presented.

Main Body

I. Photorefractivity

Photorefractivity (PR) is imparted to polymeric composites by nonlinear optical dyes that align in a space charge field, changing their refractive index. When a laser beam of the appropriate wavelength is passed through the PR material it liberates charges from the photosensitizer. The excitons created then transfer to the charge-conducting matrix. In a normal case this would just create photoconductivity (PC), but, when two beams are directed through the material and interfere with one another, a space-charge field is created with alternating light and dark areas. This is due to the difference between the PC and dark conductivity (DC) in the material, as well as the hole and electron trapping nature of some of the components. When the space-charge field is formed, it causes the nonlinear chromophores to align: one end of the chromophore tends to positive and the other to negative. This creates a grating of chromophores that would appear to oscillate from one direction to the other as one follows the space-charge field. This creates a situation in which, of the two interfering beams, one beam gains intensity while the other beam loses intensity, this change in beam intensity is the diffraction efficiency.

The alignment of the chromophores is entirely dependent on the generation and magnitude of the space-charge field, which is in turn highly dependent upon the PC characteristics of the material. By characterizing the PC properties of the material, insight into the material's PR properties can be gained as well as elucidating fundamental mechanisms involved in PR materials.

II. Synthesis of NiS Nanocrystals

All chemicals were obtained from Aldrich and used as received unless otherwise noted. Nickel sulfide nanocrystals were synthesized via an adaptation of a procedure found in the literature and all manipulations were conducted using standard airless techniques.¹⁹ In a three-neck flask, 0.48 g of $\text{NiCl}_2 \cdot 6\text{H}_2\text{O}$ were dissolved in 18 mL of oleylamine, to which was added 0.30 mL of OA, 2.7 mL of TOP, and 0.13 g sulfur flowers. The reaction proceeds immediately and the solution turns brown upon addition of sulfur, so precautions were taken to immediately begin heating the solution under vacuum. Under mechanical stirring, the solution was degassed at 100° C for approximately 1 h until the solution stopped boiling, which was assumed to be the water coordinated to the NiCl_2 . After the solution ceased boiling, the temperature was raised to 200° C and maintained at that temperature under nitrogen for 90 minutes. After 90 min the solution appeared black and was removed from heat. After allowing the solution to cool to room temperature, the nanocrystals were precipitated by the addition of ~ 10 mL of methanol. The precipitated nanocrystals were collected by centrifugation and subsequently dispersed in toluene. Several successive precipitation and dispersion cycles were conducted to remove any unreacted

constituents. The product was finally dispersed in toluene and filtered to remove large aggregates and other contaminants. Half of the dispersion was then set aside for ligand exchange.

In order to conduct the ligand exchange process on the NiS nanocrystals, the TOP/OA capped nanocrystals dispersed in toluene were precipitated once again through the addition of methanol and centrifuged. The supernatant was discarded and the wet nanocrystals were dispersed in 10 mL of pyridine. This solution was mechanically stirred overnight to allow ligand exchange. At this time the nanocrystals were precipitated through the addition of 25 mL of heptane, collected, and redispersed in pyridine. This solution was then filtered to remove any undissolved solids. Herein, the TOP/OA passivated NiS nanocrystals will be referred to as NiS:OA and those passivated with pyridine will be referred to as NiS:PY.

The NiS nanocrystals were characterized by TEM, elemental analysis, and visible absorption spectrometry. The absorption spectra were obtained using a 1 mm quartz cell at concentrations of 0.49 mg/mL for NiS:OA and 0.43 mg/mL for NiS:PY.

III. Fabrication of Photorefractive Devices

7-DCST was synthesized in our lab based on procedures described in literature.^{20, 21} For the composite samples, PVK (secondary standard), ECZ, 7-DCST, and the appropriate type and quantity of capped NiS nanocrystals were dissolved in toluene:tetrahydrofuran (2:1 by weight) and, after thorough mixing, filtered to remove any undissolved solids. This solution was stored in a vacuum oven at 50° C for 24 hours to remove the solvent and the solid residue was subsequently recovered.

Slides were prepared by etching indium tin oxide (ITO) coated glass with hydrochloric acid, producing a ¼ inch-wide and 1 ½ inch-long conducting strips. The solid was then placed between the slides and heated above its melting temperature on a hot-plate. The sample was then mechanically pressed, sandwiching the composite material between the ITO electrodes, using glass spacers to control the thickness of the device at 100 µm.

A total of six devices were fabricated, three for each type of NiS nanocrystal; NiS:OA and NiS:PY. Within each series of devices, the concentration of NiS was varied with the intention of achieving three particular device absorption coefficients at $\lambda = 633$ nm, specifically $\alpha \approx 35$ cm⁻¹, 70 cm⁻¹, and 99 cm⁻¹. For this reason, the three PR devices photosensitized with NiS:OA will herein be referred to as OA35, OA70 and OA99. Similarly, the series of three PR devices photosensitized with NiS:PY will be referred to as PY35, PY70, and PY99. The composition of each device as well as its experimentally measured absorption coefficient at $\lambda = 633$ nm is presented in Table 1. To determine the weight percentage of NiS in each composite, several NiS:solvent solutions of known absorbance and volume were evaporated to dryness and the mass of the solid residue was measured. This allowed us to correlate the absorbance and concentration in g/mL of the NiS suspensions. The weight percent of NiS in each device was thus calculated indirectly from the known absorbance and volume of the aliquot used in the fabrication of the respective composite.

IV. Photoconductivity Characterizations

Photoconductivity characterizations were made using a dc-photocurrent technique with a Keithley electrometer. The electrodes of the sample were connected to a high voltage source and placed in series with an electrometer. A zener diode was connected to the circuit to protect the

electrometer. The sample was placed so that a helium-neon (HeNe) laser operating at ~11 watts and $\lambda = 633$ nm, with a beam diameter of 0.98 mm, would be directed normal to the sample through the electrodes and material sandwiched in between.

Measurements were taken of the current flowing through the circuit with the beam blocked and unblocked at various voltages, ranging from 0 kV to 8 kV. By interpreting the dark and photo-currents, coupled with the known sample width and beam diameter, we were able to calculate the DC and PC, σ_d and σ_p respectively, as well as the quantum efficiency, Φ , of the composite material in each of the six samples at several voltages.

V. Results and Discussion

The NiS nanocrystals utilized in this study were synthesized based on a procedure found in the literature.¹⁹ Furthermore, ligand exchange was performed on the nanocrystals, replacing OA and TOP, the passivating ligands imparted to the surface of the NiS nanocrystals during the original synthesis, for pyridine. In previous studies, this procedure has been conducted in order to improve the solubility of the nanocrystals within the polymer matrix,¹⁸ however, on this occasion the optical quality of the final PR composites, as determined by light scattering experiments, was found to be excellent, independent of the passivating ligands used in this study. In the current study we use pyridine in an attempt to improve the photoconductivity and quantum efficiency of the material. It was speculated that the insulating aliphatic chains of OA and TOP would impede the electron-hole pair transfer to the charge-conducting matrix. Thus, by replacing the OA and TOP with pyridine, which due to its conjugated nature was expected to be more conducive to the electron transfer process from the nanocrystal to the conducting matrix necessary for the establishment of the space-charge field. We expected an improvement in the electronic properties of the material, resulting in improved photorefractive performance. The result however did not show improved PC but were nonetheless interesting.

Due to the dependency of the material upon the charge-generating characteristics of the nanocrystals, it was important to control the characteristics of the nanocrystals present in the composite. It was found that at temperatures given in literature, only particles were produced that did not disperse well enough in toluene to pass through a filter paper and were not optically transparent when added to the composite material. By lowering the temperature and lengthening the cooking time, nanocrystals were obtained that passed through the filter paper as a dark black solution and remained optically transparent when incorporated into the final composite material. It is also important to note that the reaction proceeds immediately upon the addition of sulfur, so care must be taken to immediately heat and degas the solution to prevent the formation of bulk NiS.

TEM was employed and the images obtained for NiS:OA and NiS:PY are presented in Fig. 1 and Fig. 2 respectively. Evident in the inset of Fig. 1 is the lattice spacing of the NiS nanocrystal, corroborating the single crystal-domain character of the NiS nanoparticles. The particles are irregularly shaped, but generally rectangular or oblong in character. Size histograms for NiS:OA and NiS:PY are presented in Fig. 3 and Fig. 4 respectively. The size histograms reflect the oblong nature of the NiS nanoparticles, illustrating both the length and width of the nanoparticles separately. For the case of NiS:OA, the mean length was determined to be 13 ± 4.2 nm ($N = 49$) and the mean width was determined as 10 ± 2.5 nm. Similarly, for the NiS:PY, the mean length was calculated to be 11 ± 3.4 nm ($N = 18$) and the mean width 8.5 ± 2.6 nm. The relatively large standard deviations are reflective of the polydispersity associated with the

nanocrystals. The data also suggests a slight reduction in the average size of the nanoparticles as a result of the pyridine treatment. This speculation was bolstered by storing NiS nanoparticles in pyridine for approximately 6 months, at the end of which time it was observed that the nanoparticles had completely dissolved into solution. Also evident in comparing Figs. 1 and 2 is that NiS:PY shows a much greater tendency for aggregation on the TEM grid. As such, achieving an accurate interpretation of the size distribution associated with the NiS:OA was uncomplicated, however, in the case of NiS:PY, only particles which could be clearly distinguished were included in the size analysis. Hence, if one sized particle has a higher propensity for aggregation over another, it is conceivable that the data obtained for NiS:PY may be skewed accordingly.

Elemental analysis was performed on the nanocrystals using EDS. For NiS:OA, the results revealed a Ni:(S) ratio of $1.0:(0.70 \pm 0.06)$. Here, it is assumed that excess Ni is present on the surface of the nanocrystal which allows attachment of the anionic OA passivating ligands. As expected, when the OA was exchanged for pyridine, the excess Ni was significantly reduced, with an ensuing Ni:(S) ratio of $1.0:(0.88 \pm 0.07)$. In this case, the neutrally charged pyridine molecules do not need to be attached to the positively charged Ni atoms on the surface of the nanocrystals. It is expected that the superfluous Ni atoms, as well as the detached OA molecules, are removed with the washing procedure following the ligand exchange process.

Visible absorption spectroscopy was performed on the NiS:OA and NiS:PY in solution and are presented in Fig. 5. Both spectra were normalized to 1 mg/mL. Looking initially at the spectra for NiS:OA, there exists a peak at 448 nm, and can be attributed to the first excitonic absorption. Given the polydisperse nature of the NiS:OA, as revealed by TEM, the presence of this clearly defined peak was unexpected. Equally remarkable was the drastic change in the appearance of the spectrum resulting from exchange of passivating ligands. Both pyridine and OA are transparent in the visible and as such, only a small blue shift was expected as a consequence of the small decrease in size of the NiS nanocrystals resulting from the ligand exchange process. Indeed there does appear to be a blue shift, with a shoulder appearing at ~ 321 nm, but there is also the emergence of a new shoulder at ~ 679 nm. This may be explained as a preferential sizing resulting from the etching known to take place during the ligand exchange process, but due to the aggregation of the NiS:PY on the TEM grid, this speculation could not be confirmed with a reasonable degree of certainty. That being said, Fig. 4 does appear to have two groupings in the lengths, with one grouping at ~ 7 nm and another at ~ 13 nm and may explain the presence of these two shoulders. The biphasic grouping is not observed in the histogram for NiS:OA.

It is also known that nanocrystals, due to their high surface to volume ratio, are highly sensitive to surface modification. In which case it is possible that changing capping ligands could have altered the absorption spectrum, although it is practically impossible to predict how this will alter the nanocrystal's absorption properties.

Also apparent in Fig. 5 is the fact that the area under the curve has increased for NiS:PY relative to that of NiS:OA, despite that both spectra are normalized to 1 mg/mL. These concentrations, however, were determined by evaporating solutions of known optical absorptions to dryness. Therefore, the masses obtained in this process also include the mass of passivating ligands as well as the any extraneous Ni which may be present. Upon exchange of the relatively massive OA and TOP ligands for the much smaller pyridine molecules, in conjunction with the loss of the additional Ni which compensated for the negatively charged OA, it is expected that although the overall mass concentrations of the respective suspensions may be equal, the

suspension of NiS:PY is actually higher in NiS concentration than that of NiS:OA. Furthermore, it has been shown that a decrease in the size of a given nanoparticle is accompanied by an increase in the oscillator strength, which would also contribute to the increase absorption cross-section.²²

PR devices were fabricated using NiS nanocrystals as the photosensitizer. The concentration of NiS nanocrystals used in each device was chosen in order to achieve a given absorption cross-section at $\lambda = 633$ nm, α_{633} . Specifically we intended to fabricate two series of devices, one series photosensitized through the inclusion of NiS:OA and the second through the inclusion of NiS:PY, with each series composed of three devices of various NiS concentration, selected such that $\alpha_{633} = 35, 70$ and 99 cm⁻¹. These α_{633} were preferred because they are representative of absorption cross-sections of all-organic PR devices common in the literature. The actual α_{633} achieved for each device are given in Table 1. Apparent from the table, for the devices photosensitized using NiS:OA, it was necessary to increase the weight percentage by a factor of ~ 1.3 relative to the devices photosensitized with NiS:PY in order to achieve a similar α_{633} . As explained earlier, this is attributed to the more massive capping ligands, in conjunction with the extra Ni required for charge compensation. As such, even though Table 1 does reflect an increase in the weight percentage of the nanocrystal used in NiS:PY photosensitized devices relative to those photosensitized through the inclusion of NiS:OA, it is assumed that the actual NiS content remains relatively constant. The absorption spectra obtained for OA35, OA70 and OA99 are presented in Fig. 6 and those acquired for PY35, PY70 and PY99 are presented in Fig.7.

A distinct characteristic feature of the PR effect is that the refractive index grating created in the medium is spatially shifted with respect to the light intensity pattern of the writing beams.²² The establishment of the grating is the result of refractive molecules aligning with the space-charge field created by the beam interference pattern in the PC medium. As a result, an asymmetric exchange of energy occurs between beams interfering in a PR medium.

As stated previously, an enhancement in the PC properties was anticipated as a result of an improvement in charge-transfer process from the nanocrystal to the charge-transport matrix necessary for the establishment of a space-charge field within the conducting medium. In order to assess this hypothesis, conductivity experiments were conducted, from which it was possible to directly determine the charge-generation quantum efficiencies, Φ , using the equation

$$\Phi = \frac{N_{cc}}{N_{ph}} = J_p \cdot \left(\frac{hc}{\lambda e \alpha d} \right), \quad (1)$$

where N_{cc} is the number of charge-carriers generated per unit volume, N_{ph} is the number of photons absorbed per unit volume, h is Plank's constant, c is the speed of light, λ is the wavelength of the incident radiation, e is the fundamental unit charge, α is the absorption coefficient of the device at λ , d is the device thickness and J_p is the experimentally determined photo-generated charge current density. The Φ measured for the devices used in this study are depicted in Fig. 8. Evident in the figure is that for a given absorption, the Φ is independent of the passivating ligand used in this study.

Also apparent from the figure is that for both NiS:OA and NiS:PY photosensitized PR devices, the Φ decreases as the concentration of nanocrystal is increased. This is an unexpected

result, as we would expect Φ to increase due to the increased density of electron generating nanocrystals.

The correlation between data in Fig. 8 also lends credence to the hypothesis that suspensions of NiS:OA and NiS:PY possessing identical absorption cross-section contain a similar number of nanocrystals despite the measure difference in residue mass and this difference being attributed for equal concentrations is due primarily to the difference in the masses of the employed passivating ligands as well as the excess Ni required to compensate for the anionic nature of the OA. This is so because the Φ is evidently quite sensitive to the nanocrystal concentration of the device. As such, the approximately equal Φ observed for OA35 and PY35 implies that the concentration of nanocrystals in the suspensions is also approximately equal despite differing concentrations by weight.

Also relevant to the PR performance of a polymeric device is the σ_p relative to the σ_d . These data are plotted for the NiS:PY photosensitized devices in Fig. 9. A similar trend was observed for the NiS:OA photosensitized devices, as evidenced in Fig. 10. The PC measurements are important in understanding the establishment of the space-charge field. The PC of a material helps separate charges by allowing charges more movement in light areas and less in dark areas. The light and dark areas created by interfering beams create the necessary positive and negative variances within the medium that cause the refractive dye molecules to align in a predictable grating.

It is interesting to note that σ_p of the NiS:OA and NiS:PY are very similar, but σ_d for the pyridine nanocrystals seems to increase much faster at a lower voltage than that of the OA/TOP capped nanocrystals. It is assumed that this behavior is due to the long nonconducting aliphatic chains of OA and TOP. Though the ligand exchange did not increase the PC or Φ of the photorefractive material, it did provide interesting data relative to conductivities of the sample which may provide useful information in the interpretation of vital PR data.

Acknowledgements

Jeffrey G. Winiarz: for his advisement in the ways of doing research.

Charles Anderson: for helping with optical characterizations.

References

- ¹*Photorefractive Materials and Their Applications, I & II, Topics in Applied Physics*, edited by P. Gunter and J.-P. Huignard (Springer-Verlag, Berlin, 1988) Vols. 61 and 62.
- ²P. Yeh, *Introduction to Photorefractive Nonlinear Optics*; (Wiley, New York, 1993).
- ³O. Ostroverkhova and W. E. Moerner, *Chem. Rev.* **104**, 3267 (2004).
- ⁴J. G. Winiarz and F. Ghebremichael, *Opt. Exp.* **12**, 2517 (2004).
- ⁵J. G. Winiarz, F. Ghebremichael, *Appl. Opt.* **43**, 3166 (2004).
- ⁶J. G. Winiarz, L. Zhang, M. Lal, C. S. Friend, and P. N. Prasad, *Chem. Phys.* **245**, 417 (1999).
- ⁷J. G. Winiarz, L. Zhang, M. Lal, C. S. Friend, and P. N. Prasad *J. Am. Chem. Soc.* **121**, 5287 (1999).
- ⁸J. G. Winiarz, L. Zhang, J. Park, and P. N. Prasad, *J. Phys. Chem. B* **106**, 967 (2002).
- ⁹J. G. Winiarz and P. N. Prasad, *Opt. Lett.* **27**, 1330 (2002).
- ¹⁰D. J. Binks, S. P. Bant D. P. West, P. O'Brien, and M. A. Malik, *J. Mod. Opt.* **50**, 299 (2003).
- ¹¹K. R. Choudhury, J. G. Winiarz, M. Samoc, and P. N. Prasad, *Appl. Phys. Lett.* **82**, 406 (2003).
- ¹²C. Fuentes-Hernandez, D. J. Suh, B. Kippelen, and S. R. Marder, *Appl. Phys. Lett.* **85**, 534 (2004).
- ¹³F. Aslam, D. J. Binks, S. Daniels, N. Pickett, and P. O'Brien, *Chem. Phys.* **316**, 171 (2005).
- ¹⁴F. Aslam, D. J. Binks, M. D. Rahn, D. P. West, P. O'Brien, N. Pickett, S. Daniels, *J. Chem. Phys.* **122**, 184713 (2005).
- ¹⁵K. R. Choudhury, Y. Sahoo, T. Y. Ohulchanskyy, and P. N. Prasad, *Appl. Phys. Lett.* **87**, 073110 (2005).
- ¹⁶K. R. Choudhury, Y. Sahoo, S. Jang, and P. N. Prasad, *Adv. Func. Mat.* **15**, 1751 (2005).

- ¹⁷N. Cho, K. R. Choudhury, R. B. Thapa, Y. Sahoo, T. Ohulchansky, A. N. Cartwright, K.-S. Lee, and P. N. Prasad *Adv. Mater.* **19**, 232 (2007).
- ¹⁸J. G. Winiarz, *J. Phys. Chem. C* **111**, 1904 (2007).
- ¹⁹A. Ghezelbash and B. A. Korgel, *Langmuir* **21**, 9451 (2005).
- ²⁰M. A. Díaz-García, D. Wright, J. D. Casperson, B. Smith, E. Glazer, W. E. Moerner, L. I. Sukhomlinova, and R. J. Twieg, *Chem. Mater.* **11**, 1784 (1999).
- ²¹P. Magdolen, Mária Mečiarová, and Štefan Toma, *Tetrahedron* **57**, 4781 (2001).
- ²²W. E. Moerner and S. M. Silence, *Chem. Rev.* **94**, 127 (1994).

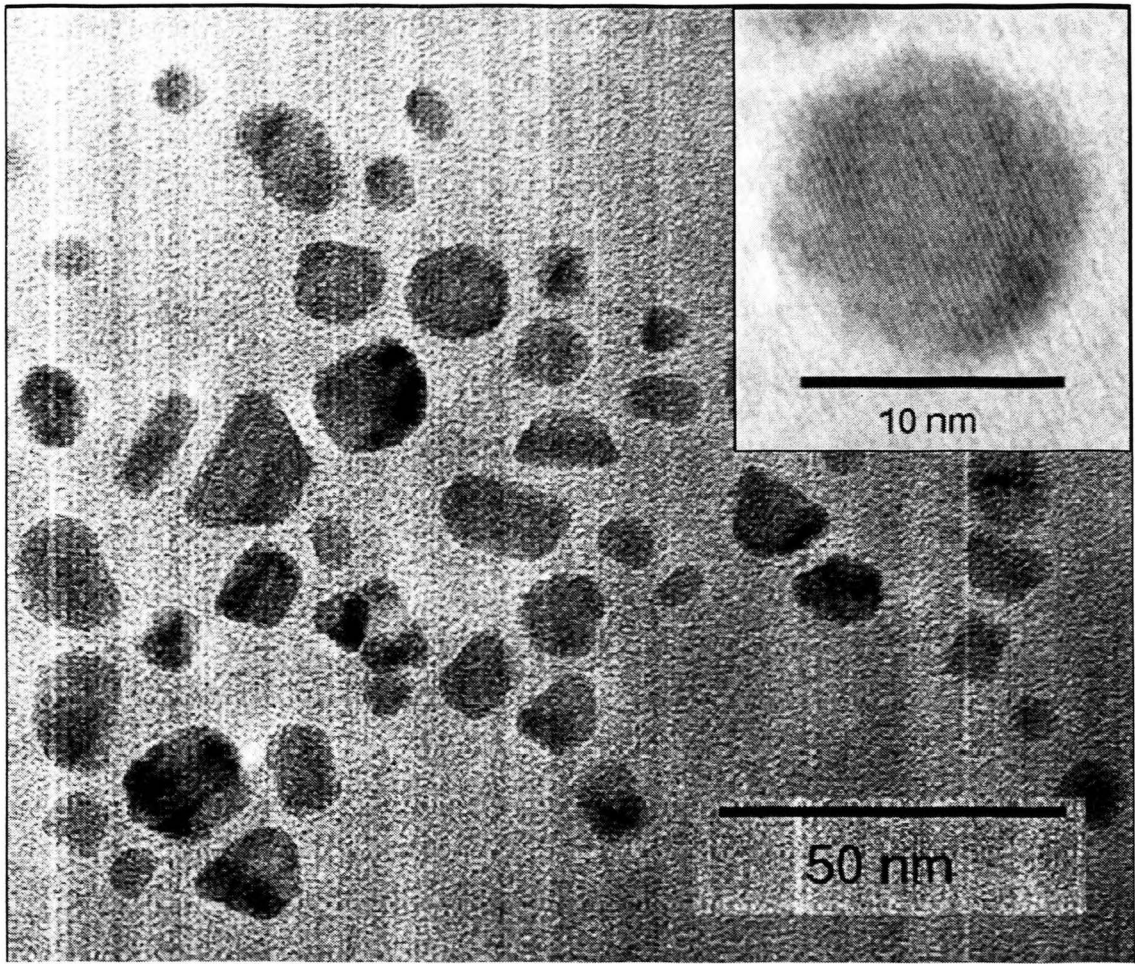


FIG. 1. TEM image of NiS:OA.

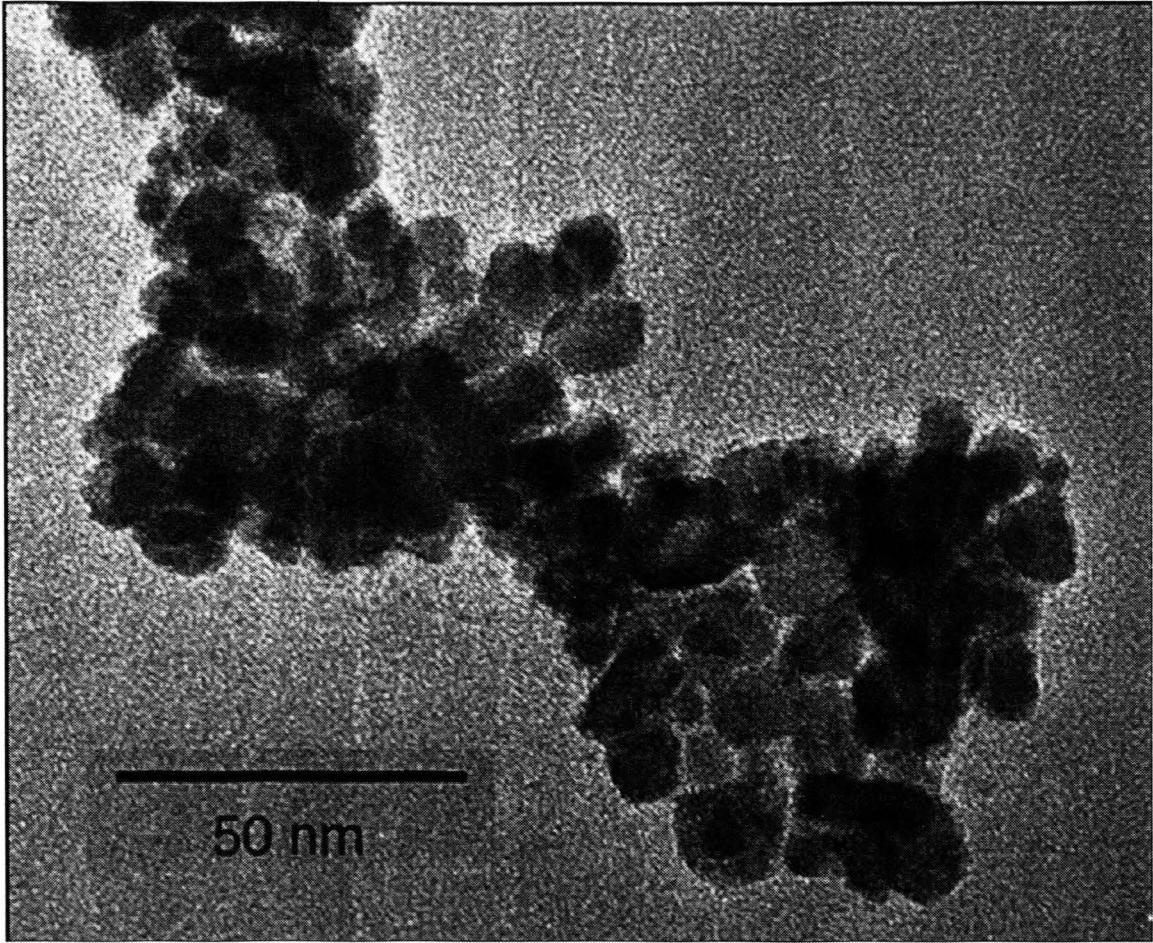


FIG. 2. TEM image of NiS:PY.

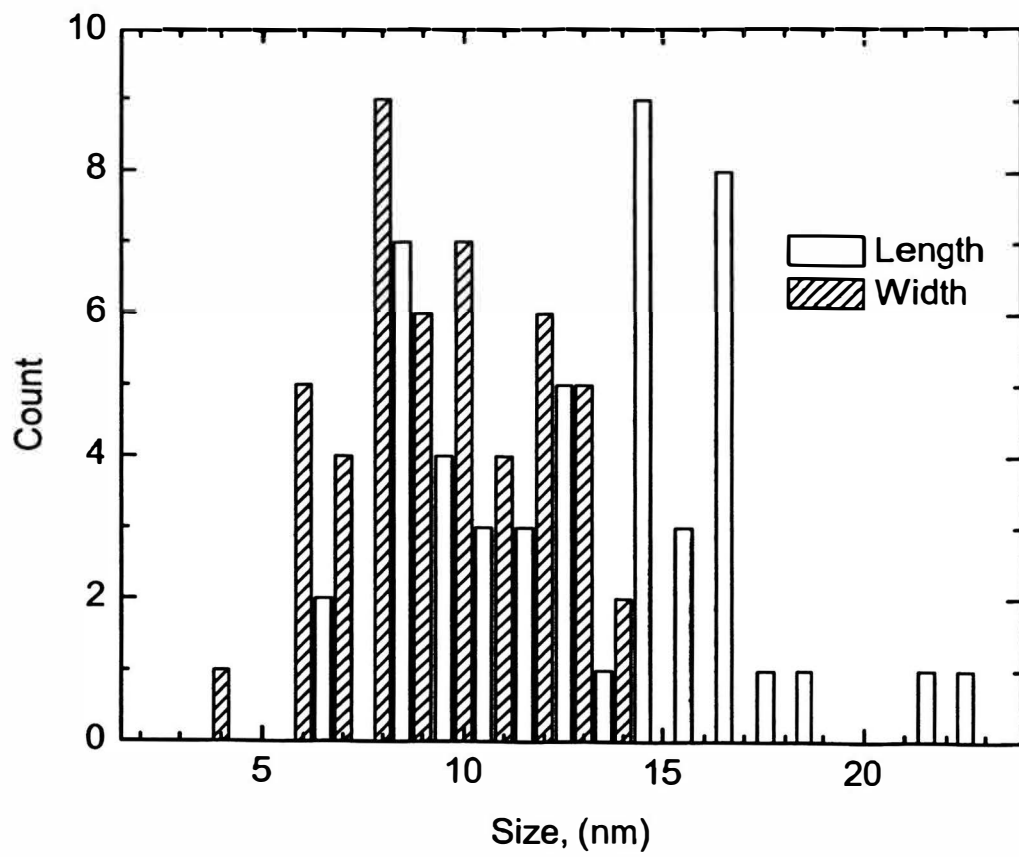


FIG. 3. Size histogram of NiS:OA.

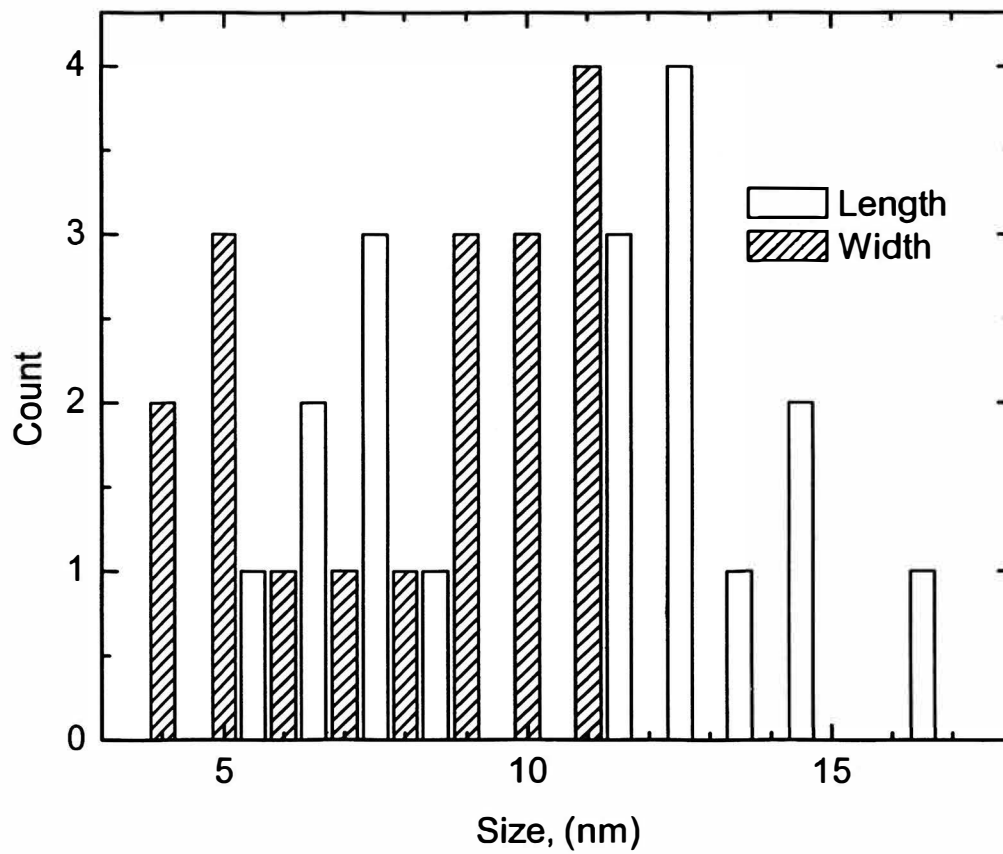


FIG. 4. Size Histogram of NiS:PY.

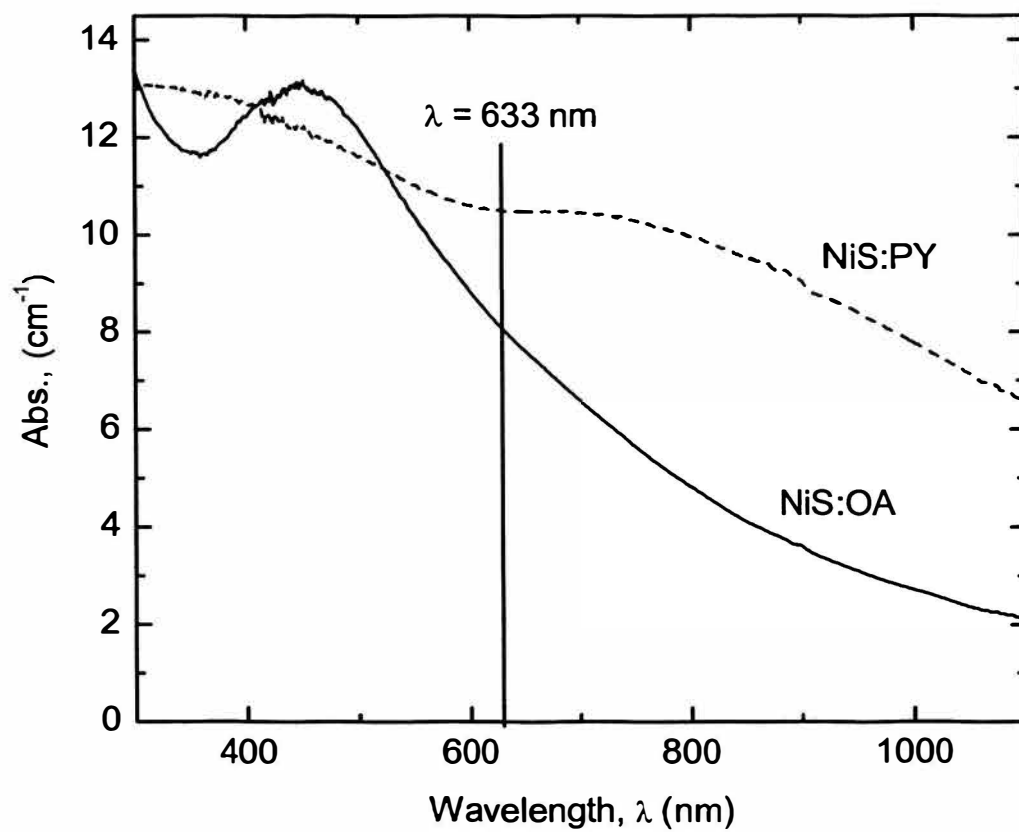


FIG. 5. Visible absorption spectra of NiS:OA (solid line) in toluene and NiS:PY (dashed line) in pyridine.

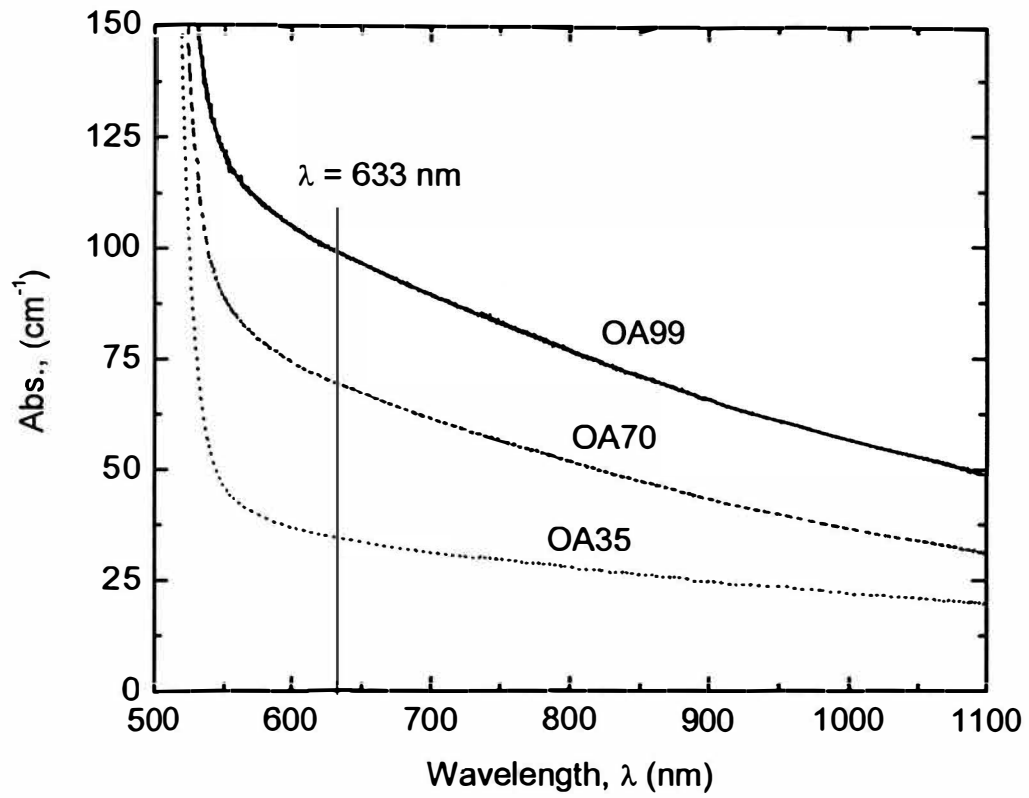


FIG. 6. Visible absorption spectra of the NiS:OA photosensitized PR devices used in this investigation; OA35 (dotted line), OA70 (dashed line), and OA99 (solid line).

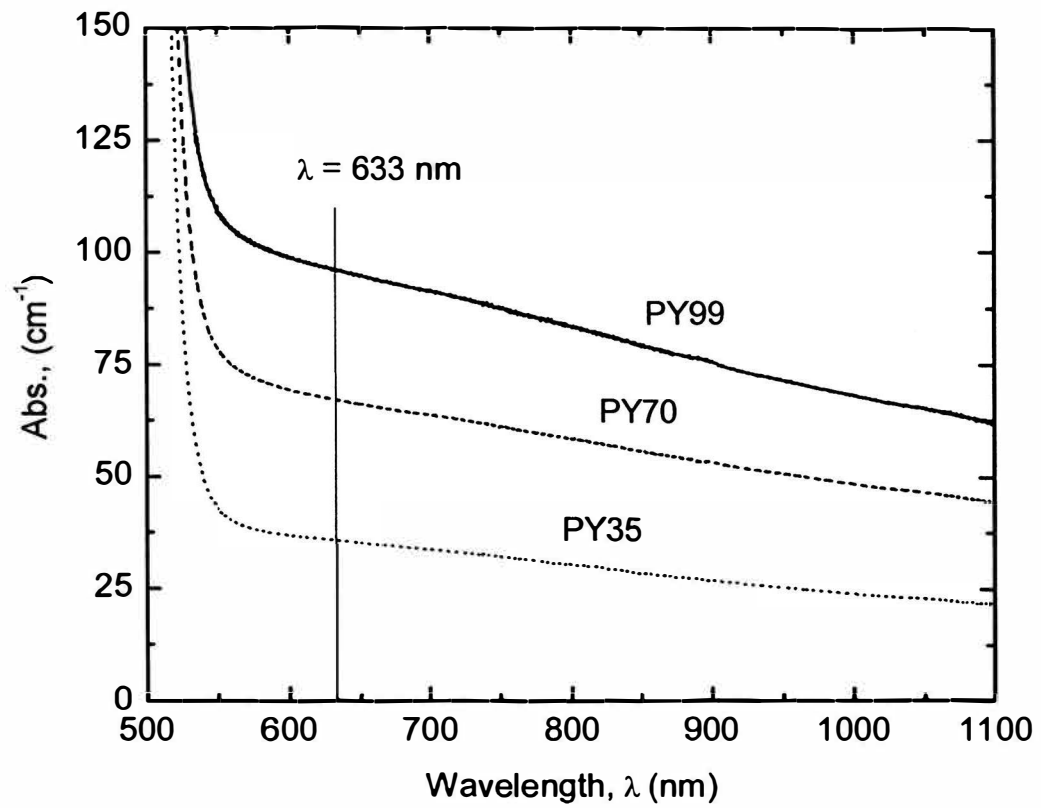


FIG. 7. Visible absorption spectra of the NiS:PY photosensitized PR devices used in this investigation; PY35 (dotted line), PY70 (dashed line), and PY99 (solid line).

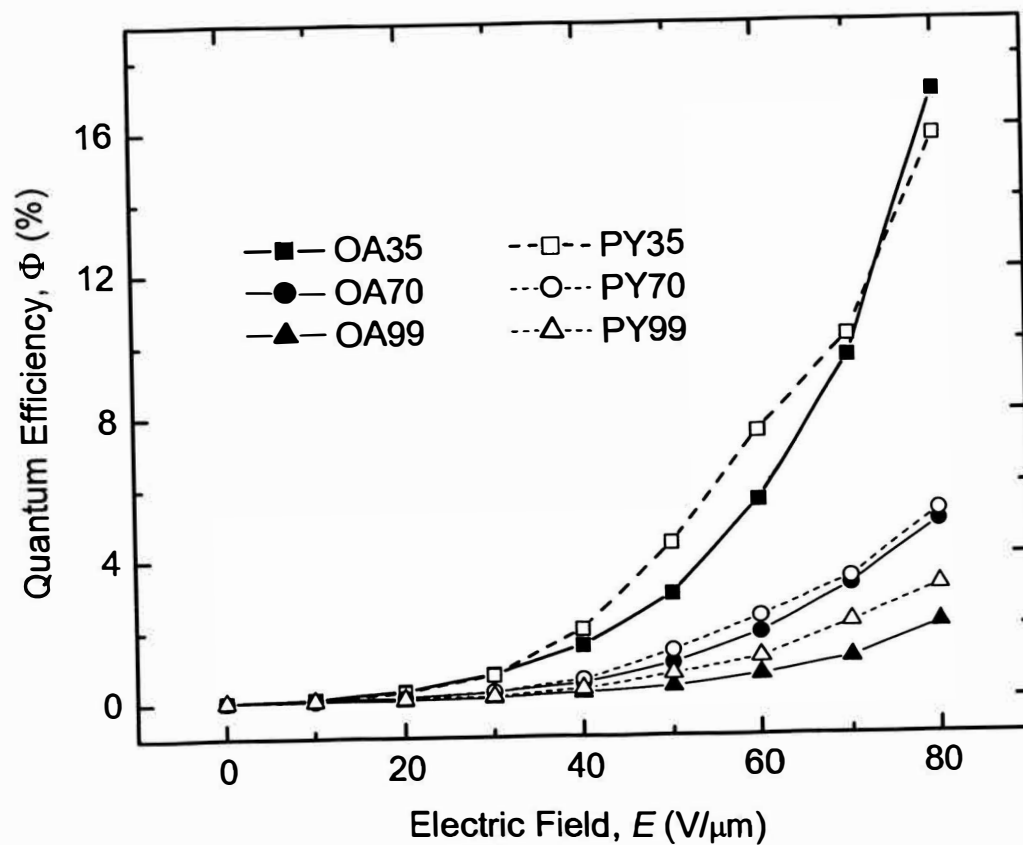


FIG. 8. Electric field dependence of the quantum efficiencies, Φ , for OA35 (solid squares), OA70 (solid circles), OA99 (solid triangles), PY35 (open squares), PY70 (open circles), and PY99 (open triangles). All data were acquired at $\lambda = 633$ nm and the lines are guides for the eye.

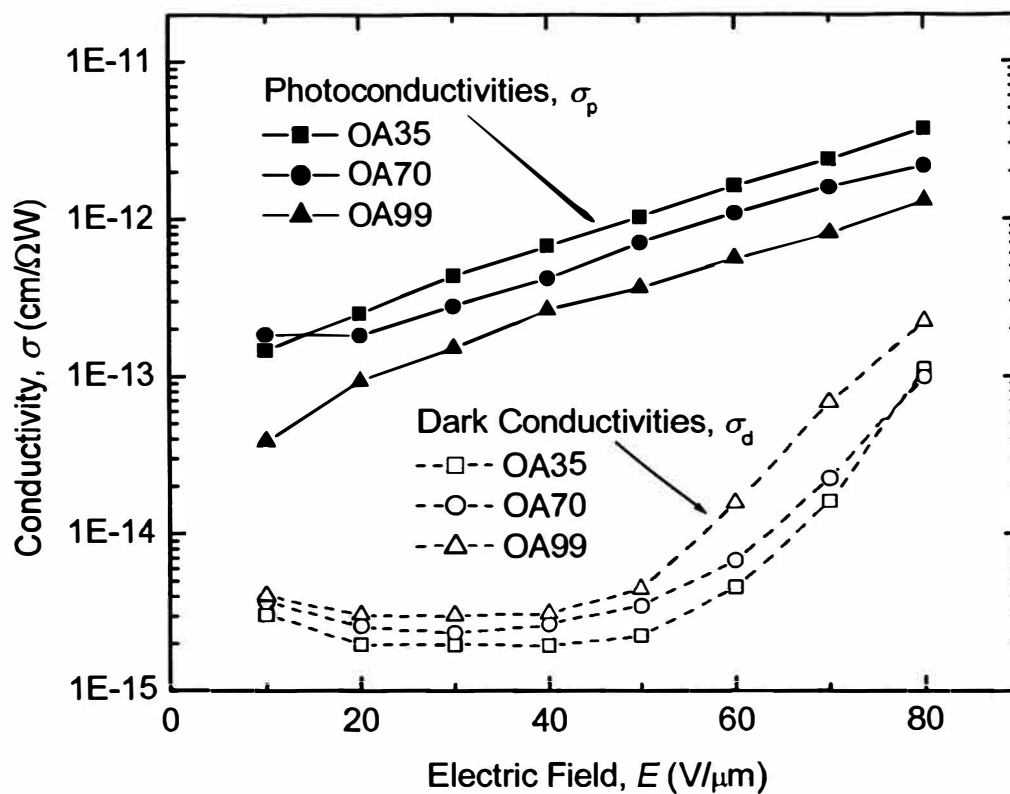


FIG. 9. Electric field dependence of the photoconductivities, σ_p , (solid symbols) and dark-conductivities, σ_d , (open symbols) of OA35 (squares), OA70 (circles), and OA99 (triangles) at $\lambda = 633$ nm. The lines are guides for the eye.

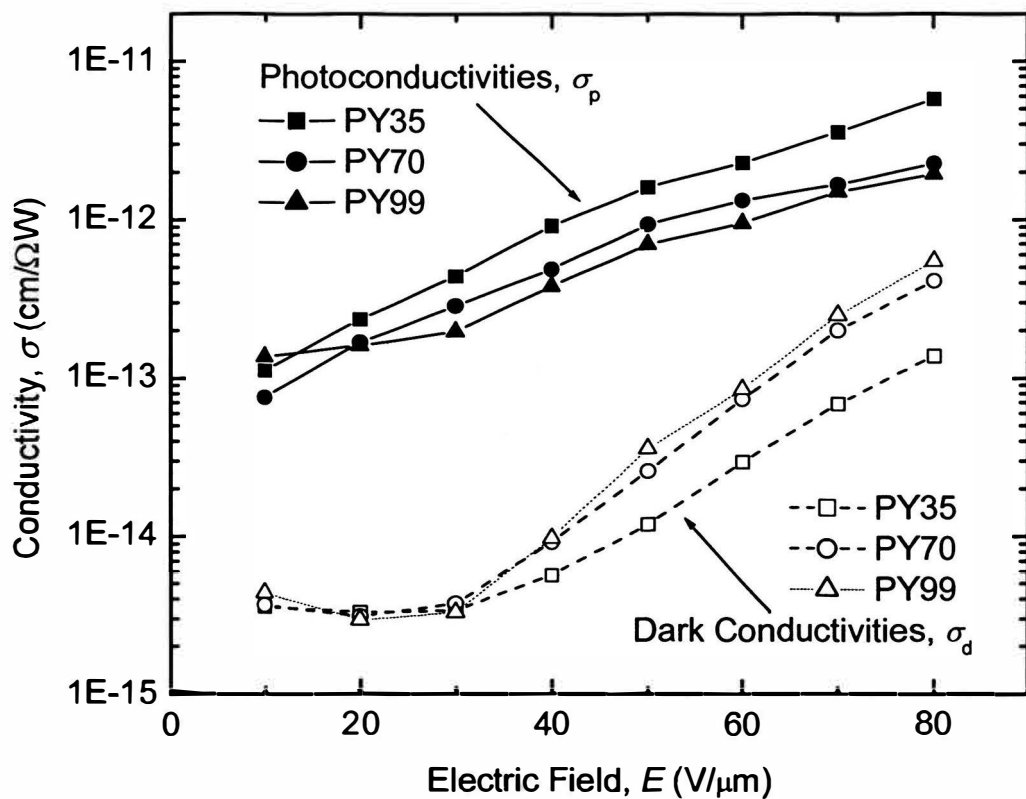


FIG. 10. Electric field dependence of the photoconductivities, σ_p , (solid symbols) and dark-conductivities, σ_d , (open symbols) of PY35 (squares), PY70 (circles), and PY99 (triangles) at $\lambda = 633$ nm. The lines are guides for the eye.